

pared with the pure elements.

Two maxima in the conduction band density of states were located with respect to the bottom of the conduction band by comparing our data for the outermost core d and p electrons for these compounds with transition energies measured by uv absorption, uv reflectivity, and electron-energy-loss experiments. One maximum is located between 0.8 and 1.4 eV above the bottom of the conduction band depending on the material and the other is located between 3 and 4 eV. This analysis showed that the higher peak was only observed in transitions from the outermost d levels of the

cation while the lower peak was observed in transitions from all of the core levels for which data were available. Both peaks correspond rather closely with the two lowest maxima which have been obtained in published density-of-states calculations for some of these compounds.

ACKNOWLEDGMENTS

We wish to thank T. C. Collins for helpful discussions. We also wish to thank B. Terrants of the U.S. Air Force Materials Laboratory for furnishing the GaP and M. Davis of the U.S. Air Force Avionics Laboratory for furnishing the GaAs.

¹C. Vesely and D. Langer, Phys. Rev. B 4, 451 (1971).

²M. Cardona, W. Gudat, B. Sonntag, and P. Yu, in *Proceedings of the Tenth International Conference on the Physics of Semiconductors, Cambridge, Massachusetts, 1970*, edited by S. Keller, J. Hensel, and F. Stern (U.S. AEC, Oak Ridge, Tenn., 1970), p. 209.

³M. Cardona, W. Gudat, E. E. Koch, M. Skibowski, B. Sonntag, and P. Y. Yu, Phys. Rev. Letters 25, 659 (1970).

⁴C. V. Festenberg, Z. Physik 227, 453 (1969).

⁵J. Helmer and N. Weichert, Appl. Phys. Letters 13, 266 (1968).

⁶D. Langer and C. Vesely, Phys. Rev. B 2, 4885 (1970).

⁷M. O. Krause (private communication).

⁸J. Bearden and A. Burr, Rev. Mod. Phys. 39, 125 (1967).

⁹F. Herman and S. Skillman, *Atomic Structure Calculations* (Prentice-Hall, Englewood Cliffs, N. J., 1963).

¹⁰F. Herman, C. Kuglin, K. Cuff, and R. Kortum, Phys. Rev. Letters 11, 541 (1963).

¹¹C. Vesely, R. Hengehold, and D. Langer, Phys. Rev. B 5, 2296 (1972).

¹²M. Cohen and T. Bergstresser, Phys. Rev. 141, 789 (1966).

¹³D. Stukel, T. Collins, and R. Euwema, in *Electronic Density of States*, edited by L. Bennett, Natl. Bur. Std. (U. S.) Spec. Publ. 323 (U. S. GPO, Washington, D. C., 1971), p. 93.

¹⁴C. Higginbotham, F. Pollak, and M. Cardona, in *Proceedings of the Ninth International Conference on the Physics of Semiconductors, Moscow, 1968* (Viniti, Moscow, 1968), p. 57.

Study of the Homology between Silicon and Germanium by Thermal-Neutron Spectrometry

G. Nilsson and G. Nelin

Aktiebolaget Atomenergi, Studsvik, Sweden

(Received 5 May 1972)

The phonon dispersion relations in silicon and germanium are found to be nearly homologous with small but significant deviations. These results, which have been obtained by thermal-neutron spectrometry, are strongly supported by an analysis in which comparison is made with elastic constants, heat capacities, and Raman frequencies for these elements. Previously observed discrepancies between results obtained from shell-model calculations and from heat-capacity measurements are explained. Attempts are made to elucidate the origin of the observed differences between the dimensionless phonon frequencies of group-IVB elements with the diamond-type crystal structure.

I. INTRODUCTION

A perturbation expansion, based on tight-binding electron wave functions in the Hartree-Fock approximation, was used by Tolpygo¹ to establish a lattice-dynamical theory for homopolar crystals of the diamond type. The equations of motion were shown by Cochran² to be equivalent to the corre-

sponding equations of the shell model; each atom is here represented by a point-ion core surrounded by a rigid spherical shell of valence electrons. In the harmonic approximation short-range forces are established by introducing spring constants allowing for core-core, core-shell, and shell-shell interactions; long-range forces are described by bare electrostatic core-core, core-

shell, and shell-shell interactions. Finally, the adiabatic approximation is obtained by assuming the electron shells to be massless. In Tolpygo's theory the vibrational frequencies $\nu_{\vec{q}j}$ (where \vec{q} is the phonon wave vector and j represents the phonon branch) are transformed into the dimensionless form

$$\Omega_{\vec{q}j} = 2\pi (\mu a^3 / e^2)^{1/2} \nu_{\vec{q}j}. \quad (1)$$

$\mu = m_1 m_2 / (m_1 + m_2)$ is the reduced mass of the atoms in a primitive unit cell, a is one-half the lattice constant, and e is the electronic charge. Equation (1) is the only combination of the quantities μ , a , and e that makes $\Omega_{\vec{q}j}$ dimensionless.

An examination of the available experimental data, such as phonon frequencies, elastic constants, and the specific heat for diamond, silicon, germanium, and gray tin, led Kucher³ to note that if the transformation expressed by Eq. (1) was applied these quantities became practically independent of which element was considered. This observation further led Kucher to postulate that the lattice dynamics of all homopolar crystals with the diamond-type structure, i. e., materials with the space-group symmetry O_h^1 are homologous to a first approximation. Thus, all the lattice-dynamical quantities appropriate to a given crystal in this group should be predictable via Eq. (1) if the corresponding quantities for another member were known. No deeper theoretical analysis of the origin of this homology was presented by Kucher.

The shell model has proved to be a good approximation for describing the lattice dynamics of ionic and covalent crystals. Thus, it requires only about ten parameters to afford an acceptable account of the phonon dispersion relations in germanium, while the Born-von Kármán model,⁴ for instance, needs almost twice this number. Moreover, the introduction of dipole-dipole interactions makes it possible to calculate the dielectric constants. In contrast to the shell model, in which the electrons are treated as being tightly bound, a large number of calculations of the electronic properties of group-IVB semiconductors (except diamond) and related solids indicate that the electrons in these crystals should be treated as nearly free (a number of references to this type of treatment are given in Ref. 5). According to the theory underlying the microscopic dielectric model,⁶ this view receives support from the fact that the values of the dielectric constants of these crystals are relatively high: $\epsilon_{Si} \approx 12$,⁷ $\epsilon_{Ge} \approx 16$,⁷ and $\epsilon_{\alpha-Sn} \approx 24$,⁸ while the value for diamond is about 6.⁹ Allowance for long-range dipole interactions is probably the main reason for the shell model needing only half as many parameters as the Born-von Kármán model. Similar considerations led Mostoller⁵ to investigate under what conditions the di-

dimensionless frequencies $\Omega_{\vec{q}j}$ will be homologous for silicon, germanium, and gray-tin crystals applying a point-ion model. In this instance the electrons are treated as a continuous gas that screens the ionic core-core interactions. It was found that for a group of materials which feature the same crystal structure and the same number of valence electrons per atom, the point-ion model yields an approximate scaling in accordance with Eq. (1) if the electron screening is weakly dependent on the electron density. This was found by Mostoller to be the case for the homopolar diamond-type crystals considered here with the exception of diamond itself.

In recent years new experimental results on phonon frequencies have been published resulting in a somewhat changed situation. Thus, the neutron-scattering experiments performed on diamond by Warren *et al.*¹⁰ revealed an appreciable difference between the phonon dispersion relations in this crystal and those in silicon,¹¹ germanium,¹² and gray tin¹³ (see Fig. 1); this not to be expected, however, from other lattice-dynamical data. The anomalous behavior of diamond may be explained by the absence of p electrons from the ionic core. The valence electrons may be expected in any case to be more localized in this material than in the others. Gray tin is, in turn, somewhat different from silicon and germanium in the sense that it is a semiconductor with zero direct band gap¹⁴ and is stable only below 286 K. Above this temperature

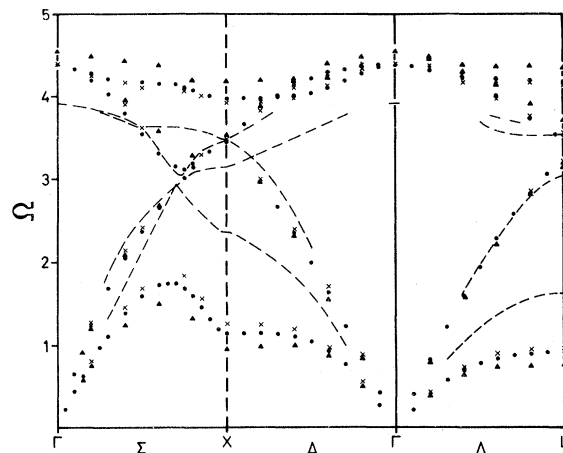


FIG. 1. Dimensionless phonon frequencies Ω for the principal symmetry directions Σ , Δ , and Λ in diamond (Ref. 10) (solid line) at 300 K; silicon (Ref. 11) (crosses) at 300 K; germanium (Ref. 12) (solid circles) at 80 K; and gray tin (Ref. 13) (solid triangle) at 90 K. The two linearly polarized branches in the Σ direction have been neglected since data are incomplete. The dispersion relations of diamond have been obtained by smoothing the data from Ref. 10.

a phase transition occurs to white tin, which has a body-centered-tetragonal crystal structure and is metallic in character. The dispersion relations of gray tin also exhibit significant differences from those of silicon and germanium, which are closely similar to each other.

An inspection of Fig. 1 reveals that the dimensionless frequencies of the two lowest branches of germanium assume somewhat lower values than do those of silicon as the zone boundary is approached. At this stage, however, these differences cannot be considered significant for the following two reasons. Firstly, the measurements were made at 80 K on germanium but at room temperature on silicon. The results could accordingly be influenced by anharmonicity although, in the temperature range considered, the effect of this factor is probably small. Secondly, it is known that the dispersion surfaces of the lowest branches in germanium form rather sharp saddle points at the reciprocal points X and L .^{12,15} At these points the frequency gradients $\nabla_{\mathbf{q}} \nu_j$ vanish making perfect focusing impossible.¹⁶ In turn, this means that as the energy and momentum resolution deteriorates, the systematic shifts toward higher frequencies become larger. There is, in fact, reason to believe that the measurements made on germanium were performed with better resolution than those made on silicon. The aim of the present experiments is to resolve the situation as regards differences between silicon and germanium. For this purpose, dispersion relations have been obtained even for branches not previously measured, but which have subsequently been found of significance in the evaluation of lattice-dynamical models.

II. EXPERIMENTAL

The experiments were carried out using the 50-MW research reactor R2 at Studsvik as a neutron source and a twin-crystal spectrometer.¹⁷ Previous results for germanium^{12,15} were obtained from measurements made with another spectrometer.¹⁸ Test runs did not demonstrate any significant differences between the present and the previously obtained frequencies, however, and the experimental results of the two spectrometers are, therefore, considered to be equivalent.

Differences between the phonon frequencies of silicon and germanium were expected to be small when scaled according to Eq. (1). The need was therefore appreciated for obtaining as nearly as possible equivalent spectrometer settings for both samples. This requirement is even greater in the instance of energy and momentum resolution. In most respects the procedures used in the present work are the same as those described in Ref. 12. Frequencies were recorded for both elements at 80 and 300 K mainly for phonons of the two lowest

branches in the three principal symmetry directions Δ , Λ , and Σ . As regards high-energy phonons only a few frequencies could be measured with high resolution, owing to inadequate focusing and insufficient neutron intensity. The limitations originate in the monochromator of the present instrument; this comprises two copper crystals adjusted to reflect neutrons only from the (220) plane. Some of the recorded phonons are shown in Fig. 2.

The silicon sample was a cylinder 20 mm in diameter and 60 mm high and with a mosaic width of less than 0.1° . The germanium crystal was about one-third of the ingot previously used.^{12,15}

TABLE I. Phonon frequencies in Si at 300 K vs reduced wave vector. a is one-half of the lattice constant, ν is in units of THz, and Ω is dimensionless.

| $(a/\pi)(q_x, q_y, q_z)$ | | | ν | Ω |
|--------------------------|-----|-----|-----------------|-------------------|
| $\Delta_5(A)$ | | | | |
| 0.1 | 0.0 | 0.0 | 1.07 ± 0.02 | 0.302 ± 0.006 |
| 0.2 | 0.0 | 0.0 | 2.02 ± 0.03 | 0.571 ± 0.009 |
| 0.3 | 0.0 | 0.0 | 2.82 ± 0.03 | 0.797 ± 0.009 |
| 0.4 | 0.0 | 0.0 | 3.47 ± 0.01 | 0.981 ± 0.003 |
| 0.5 | 0.0 | 0.0 | 3.94 ± 0.02 | 1.114 ± 0.006 |
| 0.6 | 0.0 | 0.0 | 4.22 ± 0.01 | 1.193 ± 0.003 |
| 0.7 | 0.0 | 0.0 | 4.38 ± 0.01 | 1.238 ± 0.003 |
| 0.8 | 0.0 | 0.0 | 4.47 ± 0.02 | 1.263 ± 0.006 |
| 0.9 | 0.0 | 0.0 | 4.50 ± 0.02 | 1.272 ± 0.006 |
| 1.0 | 0.0 | 0.0 | 4.51 ± 0.02 | 1.275 ± 0.006 |
| $\Lambda_3(A)$ | | | | |
| 0.1 | 0.1 | 0.1 | 1.54 ± 0.02 | 0.435 ± 0.006 |
| 0.2 | 0.2 | 0.2 | 2.63 ± 0.02 | 0.743 ± 0.006 |
| 0.3 | 0.3 | 0.3 | 3.19 ± 0.03 | 0.902 ± 0.009 |
| 0.4 | 0.4 | 0.4 | 3.37 ± 0.02 | 0.953 ± 0.006 |
| 0.5 | 0.5 | 0.5 | 3.41 ± 0.02 | 0.964 ± 0.006 |
| Σ_4 | | | | |
| 0.1 | 0.1 | 0.0 | 1.22 ± 0.01 | 0.345 ± 0.003 |
| 0.2 | 0.2 | 0.0 | 2.28 ± 0.01 | 0.644 ± 0.003 |
| 0.3 | 0.3 | 0.0 | 3.15 ± 0.01 | 0.890 ± 0.003 |
| 0.4 | 0.4 | 0.0 | 3.80 ± 0.01 | 1.074 ± 0.003 |
| 0.5 | 0.5 | 0.0 | 4.24 ± 0.01 | 1.198 ± 0.003 |
| 0.6 | 0.6 | 0.0 | 4.49 ± 0.01 | 1.269 ± 0.003 |
| 0.7 | 0.7 | 0.0 | 4.54 ± 0.02 | 1.283 ± 0.006 |
| 0.8 | 0.8 | 0.0 | 4.57 ± 0.01 | 1.292 ± 0.003 |
| 0.9 | 0.9 | 0.0 | 4.53 ± 0.01 | 1.280 ± 0.003 |
| 1.0 | 1.0 | 0.0 | 4.51 ± 0.02 | 1.275 ± 0.006 |
| $\Sigma_3(A)$ | | | | |
| 0.1 | 0.1 | 0.0 | 1.53 ± 0.01 | 0.432 ± 0.003 |
| 0.2 | 0.2 | 0.0 | 2.91 ± 0.01 | 0.823 ± 0.003 |
| 0.3 | 0.3 | 0.0 | 4.12 ± 0.01 | 1.165 ± 0.003 |
| 0.4 | 0.4 | 0.0 | 5.16 ± 0.01 | 1.458 ± 0.003 |
| 0.5 | 0.5 | 0.0 | 6.03 ± 0.02 | 1.704 ± 0.006 |
| 0.6 | 0.6 | 0.0 | 6.66 ± 0.02 | 1.882 ± 0.006 |
| 0.7 | 0.7 | 0.0 | 6.76 ± 0.06 | 1.911 ± 0.017 |
| 0.8 | 0.8 | 0.0 | 6.23 ± 0.02 | 1.761 ± 0.006 |
| 0.9 | 0.9 | 0.0 | 5.16 ± 0.02 | 1.458 ± 0.006 |
| 1.0 | 1.0 | 0.0 | 4.51 ± 0.02 | 1.275 ± 0.006 |

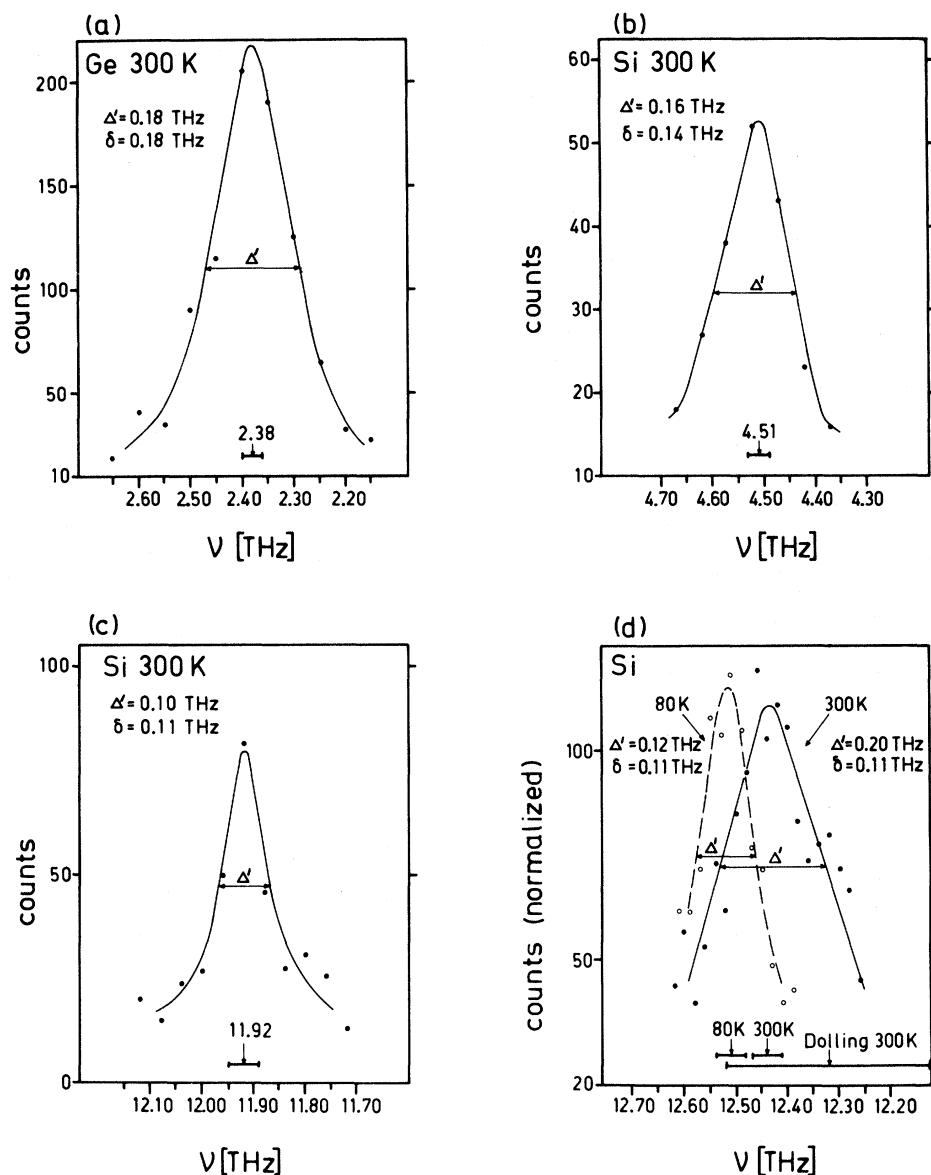


FIG. 2. Examples of phonon resonances recorded in this work: (a) X_3 in germanium at 300 K, (b) X_3 in silicon at 300 K, (c) $\Sigma_3(0)$ at (0, 6, 0) in silicon at 300 K, and (d) the temperature shift of X_1 in silicon between 80 and 300 K with the intensity at 80 K normalized to that of 300 K. δ is the calculated instrumental resolution width (Ref. 16) and Δ' (horizontal arrows) is the observed full width at half-maximum. The horizontal bars indicate the estimated errors of the frequencies.

III. RESULTS

Phonon dispersion relations have been determined in silicon at room temperature for the branches $\Delta_5(A)$, $\Lambda_3(A)$, Σ_4 , and $\Sigma_3(A)$. The frequencies of some other selected phonons have also been obtained at this temperature and at 80 K. For germanium at room temperature all frequencies were recorded at Γ , X , and L as were a few of type Σ_4 and Δ . (The nomenclature used is the

same as that used in Ref. 12.) All recorded frequencies are listed in Tables I–III, which also contain some previous results on germanium at 80 K. The frequencies of the “transverse”-acoustic branches in silicon at room temperature and in germanium at 80 K are reproduced in Fig. 3.

Quite clearly, the dimensionless acoustic frequencies of silicon lie consistently above corresponding germanium frequencies. Furthermore, this separation cannot be accounted for by the tem-

TABLE II. Miscellaneous phonon frequencies in Si at 300 and 80 K vs reduced wave vector. a is one-half of the lattice constant, ν is in units of THz, and Ω is dimensionless.

| | $(a/\pi)(q_x, q_y, q_z)$ | | | 300 K | | 80 K | |
|----------------|--------------------------|-----|-----|------------------|-------------------|------------------|-------------------|
| | | | | ν | Ω | ν | Ω |
| Δ_1 | 0.4 | 0.0 | 0.0 | 6.02 ± 0.03 | 1.701 ± 0.009 | 6.06 ± 0.02 | 1.712 ± 0.006 |
| X_3 | 1.0 | 0.0 | 0.0 | ... | ... | 4.56 ± 0.02 | 1.288 ± 0.006 |
| X_1 | 1.0 | 0.0 | 0.0 | 12.44 ± 0.03 | 3.516 ± 0.009 | 12.51 ± 0.03 | 3.535 ± 0.009 |
| $\Lambda_3(A)$ | 0.4 | 0.4 | 0.4 | ... | ... | 3.39 ± 0.02 | 0.958 ± 0.006 |
| $\Lambda_1(0)$ | 0.4 | 0.4 | 0.4 | 13.40 ± 0.04 | 3.787 ± 0.011 | ... | ... |
| L_3 | 0.5 | 0.5 | 0.5 | ... | ... | 3.43 ± 0.02 | 0.969 ± 0.006 |
| $\Sigma_3(0)$ | 0.6 | 0.6 | 0.0 | 11.92 ± 0.03 | 3.369 ± 0.009 | ... | ... |
| Σ_2 | 0.5 | 0.5 | 0.0 | 14.39 ± 0.05 | 4.067 ± 0.014 | ... | ... |
| 1 | 0.7 | 0.4 | 0.0 | 5.09 ± 0.05 | 1.439 ± 0.014 | ... | ... |

perature shift. Thus, on raising the temperature from 80 to 300 K the X_3 frequency, for example, is shifted from 1.288 to 1.275 in silicon and from 1.158 to 1.150 in germanium. The differences $\Omega_{Si} - \Omega_{Ge}$ increase with frequency to a maximum of about 10% of Ω_{Ge} at $\Omega \approx 1.5$. The difference then decreases until it becomes almost negligible at the highest optic modes. This last statement is, however, not altogether justified on the basis of the present data alone, but will be supported in Sec. IV—particularly Sec. IV A. In both materials all the measured frequencies are observed to decrease with increasing temperature. The decrease of the ordinary dimensioned frequencies is, however, greater than might be expected on the basis of volume expansion alone which indicates the influence of a nontrivial anharmonicity. Our next paper will be devoted to this subject.

In conclusion, the vibrational frequencies of germanium and silicon are to a very good approximation homologous except for the transverse-acoustic branches which show significant differences.

IV. COMPARISONS WITH OTHER DATA

A. Raman Frequency

The optical frequency Γ'_{25} can be determined with good precision in a first-order Raman scattering experiment. This has been performed for silicon by Hart *et al.*¹⁹ for the temperature range 20–770 K, by Russell²⁰ at 300 K, and for both silicon and germanium by Parker *et al.*²¹ at 300 K. The mean results at 300 K are $\Omega_{Si} = 4.408 \pm 0.004$ and $\Omega_{Ge} = 4.356 \pm 0.007$ and from neutron experiments $\Omega_{Si} = 4.389 \pm 0.065$ ¹¹ and $\Omega_{Ge} = 4.358 \pm 0.006$.¹² This gives a shift of less than 1% between Ω_{Si} and Ω_{Ge} . It is to be noted that $\Omega_{Si} > \Omega_{Ge}$. From the general behavior of the dispersion relations given in Fig. 1 the reverse order is to be expected in the absence of homology.

B. Specific Heat

In the harmonic theory of lattice dynamics²² the specific heat of a crystal at constant volume can

be expressed by

$$C_v = \sum_i x_i^2 \sinh^{-2} x_i, \quad x_i = h\nu_i / 2k_B T. \quad (2)$$

If a transformation is performed according to Eq. (1) and the reduced temperature

$$\tau = 2\pi (\mu a^3 / e^2)^{1/2} T \quad (3)$$

is introduced, Eq. (2) will be a function of the equivalent argument $X_i = h\Omega_i / 2k_B \tau$. Accurate measurement of the heat capacity of silicon and germanium at constant pressure, C_p , have been made by Flubacher *et al.*²³ in the temperature range 2.5–300 K. Plotting C_v (which is easily obtained from C_p) against τ , Kucher³ found a close numerical agreement between the C_v 's for all the materials considered here. It is our intention, however, to make a comparison more revealing of the character of silicon and germanium. A dif-

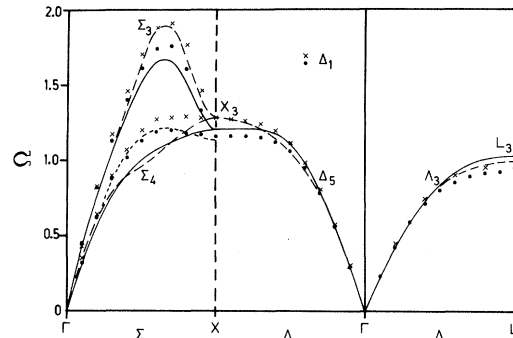


FIG. 3. Dimensionless phonon frequencies Ω below 2.0 for silicon (present work) (crosses) at 300 K and germanium (Ref. 12) (solid circle) at 80 K. The solid curves represent the results of a nine-parameter least-squares fit of the deformation-dipole model to 141 measured frequencies for germanium. The dashed curves derive from the results of Dolling's (Ref. 11) fit of an eleven-parameter shell dipole model to his silicon data, the Σ_4 branch excluded. The dotted curve has been obtained from a fit of a six-parameter valence-force potential model to 70 measured germanium frequencies. For clearer reproduction, only the results for the Σ_4 branch are presented.

TABLE III. Miscellaneous phonon frequencies in Ge at 300 and 80 K vs reduced wave vector. a is one-half of the lattice constant, ν is in units of THz, and Ω is dimensionless.

| | $(a/\pi)(q_x, q_y, q_z)$ | | | 300 K | | 80 K | |
|----------------|--------------------------|-----|-----|-----------------|-------------------|-----------------|-------------------|
| | | | | ν | Ω | ν | Ω |
| Γ'_{25} | 0.0 | 0.0 | 0.0 | 9.02 ± 0.02 | 4.358 ± 0.006 | 9.12 ± 0.02 | 4.399 ± 0.006 |
| Δ_1 | 0.3 | 0.0 | 0.0 | 2.61 ± 0.02 | 1.261 ± 0.006 | 2.59 ± 0.02 | 1.249 ± 0.006 |
| Δ_1 | 0.4 | 0.0 | 0.0 | 3.39 ± 0.02 | 1.638 ± 0.006 | 3.42 ± 0.02 | 1.650 ± 0.006 |
| Δ_1 | 0.5 | 0.0 | 0.0 | 4.15 ± 0.02 | 2.005 ± 0.006 | 4.17 ± 0.02 | 2.011 ± 0.006 |
| $\Delta_5(0)$ | 0.5 | 0.0 | 0.0 | 8.36 ± 0.03 | 4.039 ± 0.009 | 8.42 ± 0.01 | 4.061 ± 0.003 |
| Δ'_2 | 0.5 | 0.0 | 0.0 | 8.69 ± 0.03 | 4.199 ± 0.009 | 8.80 ± 0.02 | 4.245 ± 0.006 |
| X_3 | 1.0 | 0.0 | 0.0 | 2.38 ± 0.02 | 1.150 ± 0.006 | 2.40 ± 0.01 | 1.158 ± 0.003 |
| X_1 | 1.0 | 0.0 | 0.0 | 7.14 ± 0.02 | 3.450 ± 0.006 | 7.21 ± 0.01 | 3.478 ± 0.003 |
| X_4 | 1.0 | 0.0 | 0.0 | 8.17 ± 0.03 | 3.947 ± 0.009 | 8.26 ± 0.02 | 3.984 ± 0.006 |
| L_3 | 0.5 | 0.5 | 0.5 | 1.87 ± 0.02 | 0.904 ± 0.006 | 1.90 ± 0.02 | 0.916 ± 0.006 |
| L'_2 | 0.5 | 0.5 | 0.5 | 6.63 ± 0.04 | 3.203 ± 0.011 | 6.66 ± 0.02 | 3.212 ± 0.006 |
| L_1 | 0.5 | 0.5 | 0.5 | 7.27 ± 0.02 | 3.513 ± 0.006 | 7.34 ± 0.02 | 3.540 ± 0.006 |
| L'_3 | 0.5 | 0.5 | 0.5 | 8.55 ± 0.03 | 4.131 ± 0.009 | 8.70 ± 0.03 | 4.196 ± 0.009 |
| Σ_4 | 0.7 | 0.7 | 0.0 | 2.49 ± 0.02 | 1.203 ± 0.006 | 2.49 ± 0.01 | 1.201 ± 0.003 |
| Σ_4 | 0.8 | 0.8 | 0.0 | 2.44 ± 0.02 | 1.179 ± 0.006 | 2.45 ± 0.02 | 1.182 ± 0.006 |
| Σ_4 | 0.9 | 0.9 | 0.0 | 2.40 ± 0.02 | 1.160 ± 0.006 | 2.43 ± 0.01 | 1.172 ± 0.003 |

ferent approach will therefore be used which has been found to be more sensitive to the details of the lattice dynamics.

From the specific heat at constant volume, C_v , the moments defined by

$$\mu_n = \int_0^\infty \nu^n g(\nu) d\nu / \int_0^\infty g(\nu) d\nu, \quad (4)$$

where $g(\nu)$ is the phonon density of states, can be extracted.²⁴ For purposes of plotting, however, a more convenient function is

$$\nu_D(n) = [\frac{1}{3}(n+3) \mu_n]^{1/n}. \quad (5)$$

For $n=0$ and $n=-3$ we define²⁵

$$\nu_D(0) = \exp\left(\frac{1}{3} + \frac{\int (\ln \nu) g(\nu) d\nu}{\int g(\nu) d\nu}\right) \quad (6a)$$

and

$$\nu_D(-3) = (k_B/h) \Theta^c, \quad (6b)$$

respectively, where Θ^c is the heat-capacity-equivalent Debye temperature at absolute zero. The moment-equivalent dimensionless frequency $\Omega_D(n)$, defined from $\nu_D(n)$ by Eq. (1), is plotted in Fig. 4 between the limits $-3 \leq n \leq 6$ as calculated from the calorimetric data of Flubacher *et al.*²³ It is noteworthy that the main contributions to $\Omega_D(n)$ originate from different parts of the spectrum $g(\nu)$ according to which value of n is considered. This can be readily demonstrated by estimating μ_n for germanium when $n=-2$ and $+6$.

Case a ($n=-2$). In the frequency range $0 \leq \nu \leq 1.9$ THz, $g(\nu) d\nu$ can be approximated to a Debye spectrum²² (see Fig. 5). In fact a contribution $d\mu_{-2} \approx 5 \times 10^{-29} \text{ sec}^2$ is provided by an interval $d\nu = 0.01$ THz in this region. For $1.9 \leq \nu \leq 3.7$ THz and $\nu \geq 3.7$ THz typical values obtained are $d\mu_{-2} \approx 3 \times 10^{-28} \text{ sec}^2$ and $3 \times 10^{-29} \text{ sec}^2$, respectively. The

acoustic resonance region accordingly contributes about ten times more to the value $\mu_{-2} = 7.8 \times 10^{-26} \text{ sec}^2$ (value from Ref. 15) than any other region.

Case b ($n=+6$). The optic peak contributes $d\mu_6 \approx 3 \times 10^{75} \text{ sec}^{-6}$ and the acoustic peaks $d\mu_6 \approx 6 \times 10^{71} \text{ sec}^{-6}$. The ratio between these two is thus 5×10^3 . This implies that the value $\mu_6 = 1.7 \times 10^{77} \text{ sec}^{-6}$ (also from Ref. 15) is strongly dominated by contributions from the very largest frequencies.

On inspecting Fig. 4, with the above considerations in mind, it will be noticed that the $\Omega_D(n)$ curves for silicon and germanium split and that

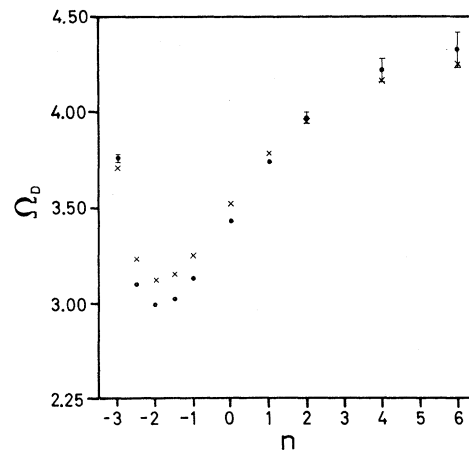


FIG. 4. Moment-equivalent, dimensionless frequency $\Omega_D(n)$, defined by Eqs. (1) and (5), for silicon (crosses) and germanium (solid circle) as calculated from the data of Flubacher *et al.* (Ref. 23). Error bars are shown for the germanium data, in instances where the dot size is exceeded.

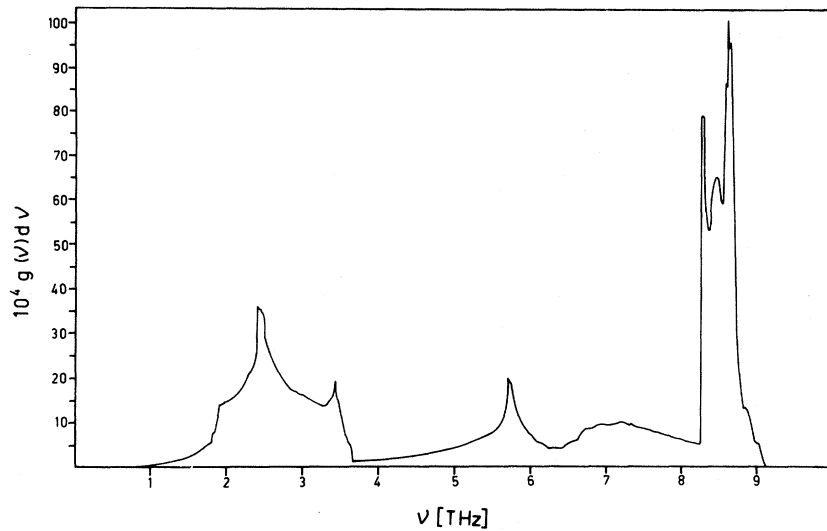


FIG. 5. Phonon density of states in germanium at 80 K as obtained by Nelin and Nilsson (Ref. 15) [$\int g(\nu) d\nu = 1$].

this splitting first increases with n , reaches a maximum for $n \approx -1.5$, and then decreases for higher values of n . For $n \geq +2$ the two curves are covered by the error bars. It has previously been shown¹⁵ that the statistical errors of the highest moments quoted for germanium by Flubacher *et al.* are likely to be overestimated by a factor of 4. On the other hand, it has been demonstrated that the highest moments, for example, μ_6 , must be sensitive even to very small differences between the dimensionless optical frequencies of the two materials. It can therefore be concluded that Ω_{S1} will, on average, be larger than Ω_{G_0} in a low-frequency region which has its center at a point corresponding to the maximum deviation at $n \approx -1.5$, i. e., somewhere in the interval $1 \lesssim \Omega \lesssim 1.5$. This is precisely what was observed in Sec. III from the results of the present experiments for the directions Δ , Λ , and Σ . Thus the observed split is likely to be present in all off-symmetry directions.

C. Elastic Constants

McSkimin²⁶ has made accurate measurements of the elastic constants in silicon and germanium in the temperature range 78–300 K. From these data it is possible to calculate elastic acoustic frequencies in the long-wavelength limit.²² The acoustic frequency gradients $d\Omega_j/dq_j$ of the Δ , Λ , and Σ directions at Γ are plotted in Fig. 6 as a function of reduced temperature τ [see Eq. (3)]; q_r is the magnitude of \vec{q} in units of π/a , and the lattice constants needed were taken from Gibbons.²⁷ The values of the derivatives $d\Omega_j/dq_r$ of practically all the branches are found to be larger for silicon than for germanium at all temperatures. Exceptions are the branches $\Delta_5(A)$ and $\Sigma_3(A)$, the derivatives of which cross at about 200 K when plotted against the ordinary temperature scale [see Fig.

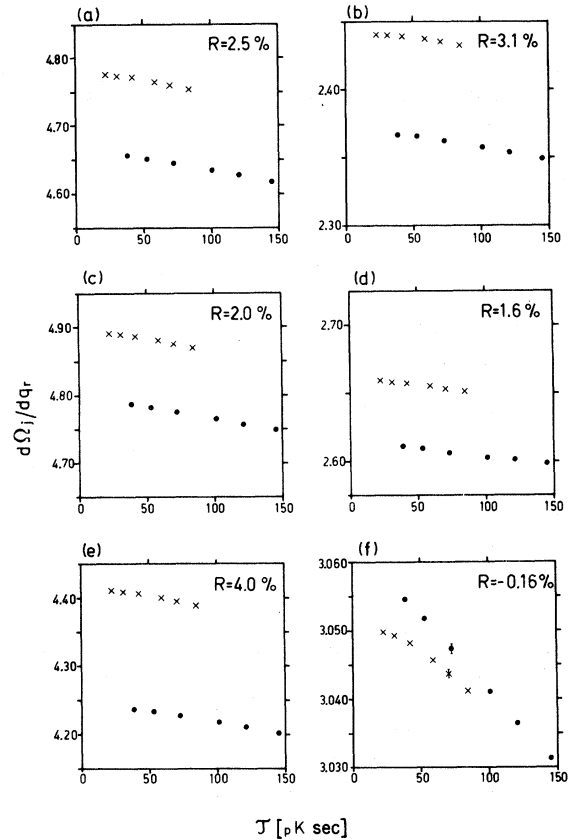


FIG. 6. Dimensionless derivatives $d\Omega_j/dq_r$ of the acoustic phonon frequencies Γ_{15} for silicon (crosses) and germanium (solid circles) as a function of reduced temperature τ . The figure shows the branches (a) $\Sigma_1(A)$, (b) Σ_4 , (c) $\Lambda_1(A)$, (d) $\Lambda_3(A)$, (e) Δ_1 , and (f) $\Delta_5(A)$ and $\Sigma_3(A)$. R is the mean percental difference between the derivatives. The requisite elastic constants were taken from the data of McSkimin (Ref. 26) at $T=80, 110, 150, 210, 250,$ and 300 K.

6f]. Thus, for small wave vectors the dimensionless acoustic frequencies for all other branches should be some percent larger in silicon than in germanium. This is in agreement with the present results expressed in Fig. 3 and Tables I-III, which even show a tendency for the $\Sigma_3(A)$ branch of silicon at 300 K to cross the corresponding branch of germanium at 80 K for small wave vectors. On the other hand, no such tendency is observed for the $\Delta_5(A)$ branch.

V. LATTICE-MODEL CALCULATIONS

The lattice dynamics of silicon and germanium have been investigated by Dolling and Cowley²⁵ who fitted a second-neighbor shell-dipole model defined by eleven parameters to experimental results obtained from Refs. 11 and 28. They, further, calculated phonon-frequency distributions (or densities of states), and derived some thermodynamic properties. An "unexplained discrepancy" observed between calculated and measured heat capacities was assumed by them to be due to defects in the model or to anharmonic effects. Their calculations also revealed a similar discrepancy in GaAs. Silicon demonstrates the most pronounced discrepancy, however, deviations between the heat-capacity equivalent Debye temperatures obtained from the shell model and from calorimetric experiments attaining a maximum of about 10% at 40 K. This indicates the possibility of a relatively large discrepancy between theory and experiment localized somewhere in the low-frequency region. Figure 3 illustrates the dispersion relations for the lowest branches in silicon as calculated by Dolling and Cowley²⁹ and in germanium. The latter curves have been derived by fitting a nine-parameter nonangular second-neighbor deformation-dipole model³⁰ to the data obtained at 80 K.¹² It should be noted, however, that the deformation model was fitted to all branches of the Δ , Λ , and Σ directions, while the shell-model fit did not include the branches Σ_2 and Σ_4 . With the exception of this Σ_4 branch the shell model affords good agreement with our silicon data. Inclusion of all the Σ branches in the deformation-model calculations merely worsened the over-all fit with the data for silicon (not shown) and germanium (Fig. 3). Both models thus give a mediocre description of the Σ_4 branch. A similar situation arises in off-symmetry directions. For example, at the point with coordinates 0.7, 0.4, 0.0 the observed values are $\Omega_{Si} = 1.439$ at 300 K and $\Omega_{Ge} = 1.375$ at 80 K; the shell-dipole model fitted to the silicon data of Dolling¹¹ predicts 1.175. These differences prove that inadequacies in the models and not anharmonic effects are responsible for the earlier mentioned discrepancies between results based on theory and on calorimetry. It is clear that, in

view of its significance, measurement of the phonon branch Σ_4 (and also Σ_2), commonly neglected by experimentalists, is essential.

Singh and Dayal³¹ and Solbrig³² fitted valence-force potential models to the experimental results for silicon obtained by Dolling¹¹ and with only six free parameters achieved as close a fit to the measured branches as that afforded by the shell model. A striking feature of the valence force calculations, however, is the prediction of a Σ_4 branch closely similar in shape to that observed in the present study. The results of a six-parameter fit to the germanium data are shown in Fig. 3.

VI. GENERAL DISCUSSION

The phonon dispersion relations of those group-IV B elements which crystallize with the diamond-type structure may be placed in one of three groups according to the changes which arise on passing from one element to the next (see Fig. 1).

The first group comprises the lowest, i. e., the "transverse"-acoustic, branches. The Σ_4 branch is reproduced in Fig. 3 but only for silicon and germanium; that for diamond,¹⁰ not included here, is situated well above the others. Data for this branch relating to grey tin¹³ are not available. If this is assumed to follow the general trend, and any eventual irregularities for very small wave vectors can be disregarded (Sec. IV C), then the shapes of the transverse-acoustic branches are found to be largely unaffected by changing the atomic species in the crystal; the frequencies are further seen to decrease with increasing atomic weight. It is noteworthy, however, that a large frequency difference exists between diamond and the other isostructural elements.

The valence-force potential model seems to account best for the transverse-acoustic branches (Sec. V). Within the framework of this model, the interactions involved can be given a simple interpretation.³² The angle-bending force F_θ , typical of a covalent bond, and the interaction force between such forces $f_{\theta\theta}$, dominate the dynamics of the branches in question. For example, there is a proportionality between the frequency X_3 (Fig. 3) and the square root of F_θ and also between L_3 and $F_\theta - f_{\theta\theta}$. Inspection of the ratio F_r/F_θ , where F_r is the bond-stretching force, shows that for silicon^{31,32} F_θ is close to $\frac{1}{50}F_r$, while for carbon in diamond and organic molecules the corresponding value is about $\frac{1}{10}F_r$.³³ As mentioned in Sec. I, calculations of the electronic properties of the semiconductors under consideration indicate that the valence electrons of silicon, germanium, and grey tin are virtually free in contrast to those of diamond. If we accept that for diamond the lack of p electrons in the carbon core leads to a higher degree of localization of the valence electrons than

is achieved in the related elements, the forces typical of covalency should be stronger in diamond. The proposed weakening of covalency is also supported by the so-called sum rule. Rosenstock³⁴ showed that the sum

$$S = \left[\sum_{i=1}^6 \nu_i^2(\vec{q}) - \sum_{i=1}^6 \nu_i^2(0) \right] / \sum_{i=1}^6 \nu_i^2(0)$$

depends on \vec{q} if nonelectrostatic forces act between second neighbors and equivalent atoms. An inspection of Fig. 7 reveals that there is in fact a strong \vec{q} dependence of S in the case of diamond, while silicon, germanium, and grey tin display weak variations with \vec{q} . It should also be noted that S is independent of the scaling of the frequencies. Accordingly, a simple explanation is provided for the behavior of the transverse-acoustic branches.

The second group comprises the intermediate frequency, i. e., "longitudinal"-acoustic branches, which show remarkably small variations as between the elements. In both the shell and valence-force potential models these branches are described by rather complicated functions of the force constants. Since the degree of homology is high, however, the results of Mostoller⁵ are directly applicable. The longitudinal-acoustic modes are then assumed to be governed by the bulk behavior of the electron gas. This is in direct contrast to the transverse-acoustic modes which are thought to be more sensitive to the actual valence electron distribution. Under these circumstances, a bulk property, such as the compressibility, can be expected to exhibit a smaller variation within the elements than a shear property, for example, a shear modulus. The elastic constants C_{ij} at room temperature^{26,35} were used to determine the

compressibility $\kappa = 3/(C_{11} + 2C_{12})$ and the shear moduli $S = \frac{1}{2}(C_{11} - C_{12})$ and $G = C_{44}$ as follows: $\kappa_{D1} = 2.27$, $\kappa_{Si} = 10.2$, and $\kappa_{Ge} = 13.3$, all in units of 10^{-13} cm²/dyn; $S_{D1} = 4.75$, $S_{Si} = 0.51$, and $S_{Ge} = 0.40$; and $G_{D1} = 5.76$, $G_{Si} = 0.79$, and $G_{Ge} = 0.67$, all in units of 10^{12} dyn/cm². No data on grey tin have been found, but neither are they altogether necessary; the above figures already support our contention. Thus the compressibility is changed by a factor of 5 while changes in the shear moduli are about 9 in magnitude as between diamond and the related elements.

The third group comprises the optical branches. The Raman frequency of diamond is much lower than that of the related elements and according to Sec. IV A the sequence runs: diamond, germanium, silicon; a succession which appears anomalous. In the deformation-dipole model³⁰ the Raman frequency is almost entirely determined by the force constant G (not to be confused with shear modulus G). This describes parts of the interaction between two unperturbed nearest-neighbor atoms, i. e., in the absence of dipole moments. (It is also closely related to the elastic constant C_{11} .)

While the general behavior of the optical branches is more difficult to interpret, one detail is worthy of notice. The dimensionless frequency of the lowest optical branch at L , i. e., the longitudinal L_1 , is practically identical for these isostructural elements excepting grey tin. In the valence-force potential model³² this frequency is proportional to the square root of F_r , the bond-stretching force constant, which should thus be homologous to a high degree. Unfortunately, there are no other data to support this statement.

To summarize, it would seem that the lattice dynamics of diamond, silicon, germanium, and grey tin are closely similar, though not quite homologous in the sense used by Kucher.³ To a first approximation the transverse-acoustic modes are lowered and corresponding longitudinal modes remain constant while optic modes in general increase as the atomic weight of the element increases. Dependence on the valence-electron distribution in these elements seems to be an important feature of their lattice dynamics. A reasonable conclusion from the above discussion is that the observed differences are closely related to changes in the degree of metallization realized on passing from one element to the next. This property is another way of expressing the actual degree of extension of non-core-electron orbitals. An example is given by the direct energy gap between the valence and conduction bands, which is 5.4 eV in diamond,³⁶ 1.19 eV in silicon,⁷ 0.77 eV in germanium,⁷ and about 0 eV in grey tin¹⁴; the ratio of the differences between these values is 10 : 1 : 1.8. The weakening covalency is described

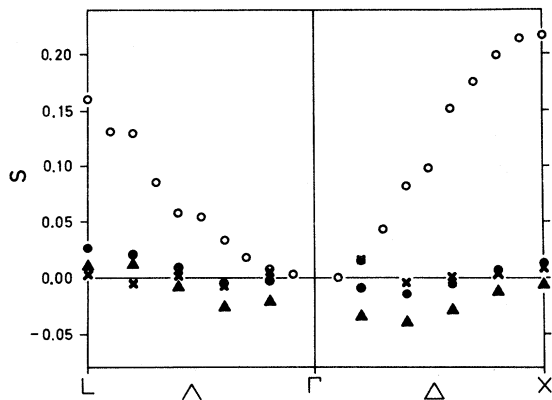


FIG. 7. $S = [\sum_{i=1}^6 \nu_i^2(\vec{q}) - \sum_{i=1}^6 \nu_i^2(0)] / \sum_{i=1}^6 \nu_i^2(0)$ for the directions Δ and Λ for diamond (Ref. 10) (open circle), silicon (Ref. 11) (crosses), germanium (Ref. 12) (solid circle), and grey tin (Ref. 13) (solid triangle). The Σ direction is not included since data are incomplete. The mean absolute errors are estimated to be 0.02.

by the change in the angle-bending force constant F_θ in the valence-force potential model; this constant governs the frequency of the transverse-acoustic mode X_3 . With reference to the ratios mentioned above, it should be noted that the differences between the dimensionless frequencies

Ω_{x_3} conform to a closely similar pattern, the ratio being 8.8 : 1 : 1.7.

ACKNOWLEDGMENT

The authors are indebted to Dr. J. M. Rowe for valuable discussions on the present work.

¹K. B. Tolpygo, *Fiz. Tverd. Tela* **3**, 943 (1961) [*Sov. Phys. Solid State* **3**, 685 (1961)].

²W. Cochran, *Proc. Roy. Soc. (London)* **A253**, 260 (1959).

³T. I. Kucher, *Fiz. Tverd. Tela* **4**, 2385 (1962) [*Sov. Phys. Solid State* **4**, 1747 (1963)].

⁴F. Herman, *J. Phys. Chem. Solids Suppl.* **8**, 405 (1959).

⁵M. Mostoller, *J. Phys. Chem. Solids* **31**, 307 (1970).

⁶R. M. Martin, *Phys. Rev.* **186**, 871 (1969).

⁷H. Y. Fan, in *Solid State Physics*, edited by F. Seitz and D. Turnbull (Academic, New York, 1955), Vol. 1, p. 283.

⁸R. E. Lindquist and A. W. Ewald, *Phys. Rev.* **135**, A191 (1964).

⁹*Physical Properties of Diamond*, edited by R. Berman (Clarendon, Oxford, 1965).

¹⁰J. L. Warren, J. L. Yarnell, G. Dolling, and R. A. Cowley, *Phys. Rev.* **158**, 805 (1967).

¹¹G. Dolling, in *Inelastic Scattering of Neutrons in Solids and Liquids* (IAEA, Vienna, 1963), Vol. II, p. 37.

¹²G. Nilsson and G. Nelin, *Phys. Rev. B* **3**, 364 (1971).

¹³D. L. Price and J. M. Rowe, *Solid State Commun.* **7**, 1433 (1969).

¹⁴S. Groves and W. Paul, *Phys. Rev. Letters* **11**, 194 (1963).

¹⁵G. Nelin and G. Nilsson, *Phys. Rev. B* **5**, 3151 (1972).

¹⁶R. Stedman, *Rev. Sci. Instr.* **39**, 878 (1968).

¹⁷R. Stedman, L. Almqvist, G. Raunio, and C. Nilsson, *Rev. Sci. Instr.* **40**, 249 (1969).

¹⁸R. Stedman and G. Nilsson, *Rev. Sci. Instr.* **39**, 637 (1968).

¹⁹T. R. Hart, R. L. Aggarwal, and B. Lax, *Phys. Rev. B* **1**, 638 (1970).

²⁰J. P. Russell, *Appl. Phys. Letters* **6**, 223 (1965).

²¹J. H. Parker, Jr., D. W. Feldman, and M. Ashkin, *Phys. Rev.* **155**, 712 (1967).

²²M. Born and K. Huang, *Dynamical Theory of Crystal Lattices* (Oxford U. P., London, 1954).

²³P. Flubacher, A. J. Leadbetter, and J. A. Morrison, *Phil. Mag.* **4**, 273 (1959).

²⁴T. H. K. Barron, W. T. Berg, and J. A. Morrison, *Proc. Roy. Soc. (London)* **A242**, 478 (1957).

²⁵G. Dolling and R. A. Cowley, *Proc. Phys. Soc. (London)* **88**, 463 (1966).

²⁶H. J. McSkimin, *J. Appl. Phys.* **24**, 988 (1953).

²⁷D. F. Gibbons, *Phys. Rev.* **112**, 136 (1958).

²⁸B. N. Brockhouse and P. K. Iyengar, *Phys. Rev.* **111**, 747 (1958).

²⁹We are indebted to Dr. G. Dolling for sending us the actual figures of his calculations.

³⁰Z. A. Demidenko, T. I. Kucher, and K. B. Tolpygo, *Fiz. Tverd. Tela* **3**, 2482 (1961) [*Sov. Phys. Solid State* **3**, 1803 (1962)].

³¹B. D. Singh and B. Dayal, *Phys. Status Solidi* **38**, 141 (1970).

³²A. W. Solbrig, Jr., *J. Phys. Chem. Solids* **32**, 1761 (1971).

³³H. L. McMurry, A. W. Solbrig, Jr., J. K. Boyter, and C. Noble, *J. Phys. Chem. Solids* **28**, 2359 (1967).

³⁴H. B. Rosenstock, *Phys. Rev.* **129**, 1959 (1963).

³⁵H. J. McSkimin and W. L. Bond, *Phys. Rev.* **105**, 116 (1957).

³⁶C. D. Clark, *J. Phys. Chem. Solids* **8**, 481 (1959).

Reflectivity of $\text{ZnSe}_x\text{Te}_{1-x}$ Single Crystals

Atsuko Ebina, Mitsuo Yamamoto, and Tadashi Takahashi
Research Institute of Electrical Communication, Tohoku University, Sendai 980, Japan
 (Received 28 January 1972)

Reflectivity spectra of $\text{ZnSe}_x\text{Te}_{1-x}$ single crystals were measured from 2.0 to 6.6 eV through the whole range of mole fraction x at room temperature. The variation of the band gaps such as the E_0 , e_1 , E_1 , and E_2 with x is reported. The E_0 , e_1 , and E_1 gaps exhibit spin-orbit splitting. The lowest gap E_0 shows a minimum in energy at $x=0.33$. The minimum value is 2.13 eV.

I. INTRODUCTION

Since an early report by Larach *et al.*¹ on the diffuse reflectance of the microcrystalline powders of the ZnSe-ZnTe system, few papers have reported

on the variation of the band gaps with composition. The variation of the lowest band gap with composition in the $\text{ZnSe}_x\text{Te}_{1-x}$ alloys has been investigated by the crystal color observed under a microscope² and by the reflection spectra.³ Aven *et al.*⁴ have